Raman fingerprint of chromate, aluminate and ferrite spinels

Journal of RAMAN SPECTROSCOPY

Raman fingerprint of chromate, aluminate and ferrite spinels

Journal:	*Journal of Raman Spectroscopy*
Manuscript ID:	JRS-15-0087.R2
Wiley - Manuscript type:	Research Article
Date Submitted by the Author:	n/a
Complete List of Authors:	D'Ippolito, Veronica; Sapienza, University of Rome, Earth Sciences Andreozzi, Giovanni; Sapienza, University of Rome, Earth Sciences Bersani, Danilo; University, Physics and Earth Sciences Lottici, Pier Paolo; University, Physics and Earth Sciences
Keywords:	Spinel, Solid solution, Chromate , Aluminate, Ferrite

Raman fingerprint of chromate, aluminate and ferrite spinels

Veronica D'Ippolito,[a*] Giovanni B. Andreozzi,[a] Danilo Bersani,[b] Pier Paolo Lottici[b]

[a]Department of Earth Sciences, Sapienza University, Piazzale Aldo Moro 5, 00185, Rome, Italy

[b]Department of Physics and Earth Sciences 'M. Melloni', University of Parma, Parco Area delle Scienze 7/a, 43124 Parma, Italy

*Correspondence to: Veronica D'Ippolito, Department of Earth Sciences, Sapienza University, Piazzale Aldo Moro 5, 00185, Rome, Italy.
E-mail address: veronica.dippolito@uniroma1.it

Abstract

Synthetic and natural spinel single crystals having compositions closely approaching spinel end-members $ZnCr_2O_4$, $MgCr_2O_4$, $FeCr_2O_4$, $ZnAl_2O_4$, $MgAl_2O_4$, $CoAl_2O_4$, $FeAl_2O_4$, $MnAl_2O_4$, $MgFe_2O_4$ and $FeFe_2O_4$ were investigated by Raman spectroscopy in the 100-900 cm^{-1} range using both the red 632.8 nm line of a He-Ne laser and the blue 473.1 nm line of a solid state Nd:YAG laser.

Each end-member exhibits a Raman fingerprint with at least one peculiar peak in terms of Raman shift and relative intensity. Chromates and ferrites exhibit the most intense A_{1g} mode at around 680 cm^{-1}, at lower wavenumbers than in the aluminates, in agreement with the heavier atomic mass of Cr and Fe with respect to Al. For aluminate spinels the most intense and diagnostic peaks in the spectrum are: $F_{2g}(1)$ at 202 cm^{-1} for $MnAl_2O_4$, E_g at 408 cm^{-1} for $MgAl_2O_4$, $F_{2g}(2)$ at 516 cm^{-1} for $CoAl_2O_4$, $F_{2g}(3)$ at 661 cm^{-1} for $ZnAl_2O_4$ and A_{1g} at 748 cm^{-1} for $FeAl_2O_4$. Noteworthy, analysing the A_{1g}, $F_{2g}(3)$, and, in particular, the E_g peak positions, it is possible to establish which sub-group a spinel belongs to, and a careful inspection allows determination of the end-member type.

Introduction

Spinel minerals and materials belong to a large group of compounds with cubic symmetry (space group $Fd\bar{3}m$) and have the general chemical formula AB_2X_4, where A and B are cations with variable valence and X is the anion, which can be O^{2-}, S^{2-}, Se^{2-} or Te^{2-}.[1,2] Spinel-type structure is based on an approximately cubic close packing of anions, with cations hosted within tetrahedrally (T) and octahedrally coordinated (M) sites. In general, A and B cations can reside on both T and

M sites, thus giving rise to a variable disorder degree, which can be described using the inversion parameter *i*, defined as the fraction of the *B* cations at the T sites. The inversion parameter can therefore vary from 0, in the completely normal spinel $^{T}A^{M}B_2X_4$, to 1, in the completely inverse spinels $^{T}B^{M}(AB)X_4$, assuming the value 2/3 for a completely random (i.e. disordered) cation distribution.

The flexibility in the range of cations and cation charge combinations hosted in the spinel structure makes it a versatile structure adopted by over a hundred compounds, important as both minerals and synthetic materials.

Thanks to their quite simple structure and extremely diversified physical properties, synthetic compounds having spinel-type structure are used in many branches of the materials science for a large variety of applications: from semi-conductors to catalysts, from refractory materials to electrode for batteries, from magnetic devices to pigments.[3-6]

Natural spinels are frequent in most geological environments and occur as main or accessory minerals in different rocks in the Earth's lower crust and upper mantle. Being the cation distribution highly sensitive to temperature, pressure, oxygen fugacity and bulk rock and fluid composition, its full knowledge is extremely useful for constructing mineral geothermometers, geobarometers and oxygen fugacity sensors for petrologic studies.[7-12] Spinel minerals have been also discovered in extraterrestrial materials, as for example in Martian meteorites. The identification and compositions of the spinels on Mars provide information and constraints on conditions of rock genesis and alteration. In addition, they can provide evidence for magnetism on the "red planet" and can give information about oxygen fugacity and the possibility of life on Mars.[13-15] Besides geological implications, natural spinels have been appreciated as attractive and brilliant gemstones for centuries for their wide palette of vivid colors, from red to pink, violet to lavender and light blue to green.[16,17]

Raman spectroscopy is a technique widely used for routine identification of materials and its application to spinels is extremely promising. It may allow distinguishing the spinel species from the characteristic spectral patterns ('fingerprinting'), without any preliminary information about composition and structural origin of the individual features. For such reasons, Raman spectroscopy has been used for routine investigation of spinel species in materials science, cultural heritage, mineralogy, geology, gemology and play an important role also in

astromineralogy for the characterization of mineralogical and organic materials during the future exploration of Mars.[13,18-21]

Considering the numerous cations that the spinel structure can host, the number of potential Raman spectra is very large. Several catalogues and some database of Raman spectra of mineral species have been already published and are free on the Web, as for example RRUFF Project,[22] Minerals Raman Database,[23] Handbook of Minerals Raman Spectra[24] and RASMIN.[25] However, the catalogues above reported include only few spinel end-members. In addition, there has been a large amount of experimental and theoretical Raman studies on spinels but they are often focused on the most common spinels (e.g. spinel *s.s.*) and/or on specific topics such as the variations of Raman spectra with pressure, temperature and ordering.[26-35] To our knowledge, a systematic and comparative Raman study on different spinel end-members is still lacking in literature.

In this study, ten spinel single crystals, having compositions approaching chromate, aluminate and ferrite spinel end-members, have been investigated to identify Raman peculiarities of each end-member and clarify how substitution of the divalent and trivalent cations affects the Raman modes.

Materials and methods

Ten spinel single crystals were examined by Raman spectroscopy: eight synthetic and two natural spinels. All synthetic samples were synthesized by the flux growth method and chemically analyzed by electron microprobe.[36-40] These samples showed a composition very close to the spinel end-members $ZnCr_2O_4$, $MgCr_2O_4$, $FeCr_2O_4$, $MgAl_2O_4$, $CoAl_2O_4$, $FeAl_2O_4$, $MnAl_2O_4$ and $MgFe_2O_4$. The Raman spectrum of a natural magnetite coming from the Jacupiranga Complex (Brazil) was recorded. Magnetites from this site have been widely investigated by Gaspar and Wyllie[41] and showed a composition closely to the magnetite ($FeFe_2O_4$) end-member with the $FeFe_2O_4$ content ranging from 50 to 98%. In addition, the Raman spectrum of a natural sample, labelled Ni8967c, closely approaching the gahnite ($ZnAl_2O_4$) end-member, already recorded by D'Ippolito et al.,[42] was considered in the comparison among the different end-members. Chemical results of each sample are reported in Table 1. The labels used by the authors mentioned above are reported for each spinel end-member. Regarding the magnetite, electron microprobe analyses were performed on natural single crystals mounted in polished and carbon-

coated epoxy discs at CNR-IGAG lab c/o Sapienza University of Rome with a wavelength-dispersive X-ray spectrometry (WDS) on a Cameca-Camebax SX50 instrument operating at an accelerating potential of 15 kV and a sample current of 15 nA, with an incident beam size of ~1 μm. Natural standards used were corundum (Al), magnetite (Fe), rhodonite (Mn) and periclase (Mg). A PAP CAMECA program was used to convert X‑ray counts into weight percentages of the corresponding oxides.

Raman spectroscopy

Raman spectroscopy was performed on single crystal samples in nearly backscattered geometry using a Jobin-Yvon Horiba LabRam microRaman apparatus. An Olympus microscope with ×10, ×50 and ×100 objectives was used to focus on the samples. The spectra were recorded at room temperature using the excitation of both the red 632.8 nm line of a He-Ne laser and the blue 473.1 nm line of a solid state Nd:YAG laser.

Iron spinels were investigated with the red 632.8 nm line to avoid the laser-induced oxidation to haematite. The spectra of the other end-member spinels were recorded with the lower wavelength blue laser to avoid the Cr fluorescence often acquired with the red laser. By means of filters the laser power was reduced to <1 mW on the sample in order to avoid heating effects. The wavenumber calibration was performed using the 520.6 cm^{-1} Raman peak of silicon before each experimental session. The spatial resolution was ~1-2 μm, whereas the spectral resolution ranged between 2 and 3 cm^{-1} depending on the laser source. No attempt was made to measure oriented crystals. The spectra, with counting times in the range 30 - 120 s, were collected on the same crystals used for the chemical investigation, after removing the carbon layer, to allow a precise correlation between Raman spectra and chemistry for each sample.

The peak positions were obtained from baseline-corrected spectra by least-squares spectral peak-curve fitting using the Labspec® software. A Lorentzian profile was used in the peak-profile analysis. At least five spectra were collected at different positions within the sample and the resulting spectra were found to be nearly identical.

Results and discussion

In the spinel structure (space group O_h), when the origin of the unit cell is taken at the center of symmetry ($\bar{3}m$), the cations are fixed at special positions 8a (T) and 16d (M) at 1/8, 1/8, 1/8 and

1/2 1/2 1/2 fractional coordinates, respectively. The anions also occupy a special position, 32e, with 3m symmetry but with a variable fractional coordinate (u,u,u). However, although 56 atoms are present within the spinel unit cell, only 14 atoms are necessary to construct the simplest primitive cell. Group theory analysis at **k**=0,[43] predicts the following 42 vibrational modes in the spinels, 3 acoustic modes and 39 optical modes:

$$A_{1g}(\mathrm{R}) + E_g(\mathrm{R}) + F_{1g} + 3F_{2g}(\mathrm{R}) + 2A_{2u} + 2E_u + 5F_{1u}(\mathrm{IR}) + 2F_{2u}$$

Where the (R) and (IR) identify Raman- and infrared-active vibrational species, respectively, and the rest of the modes are acoustic or silent modes. The $E_{g,u}$ and $F_{1g,2g,1u,2u}$ modes are doubly and triply degenerate, respectively. The three acoustic modes belong to F_{1u} species.
In detail, the irreducible representations that describe the normal modes of vibration associated with each atomic species in their Wyckoff positions are:

8a [T]: $F_{1u}(\mathrm{IR}) + F_{2g}(\mathrm{R})$
16d [M]: $A_{2u} + E_u + F_{2u} + 2F_{1u}(\mathrm{IR})$
32e [X]: $A_{1g}(\mathrm{R}) + A_{2u} + E_u + E_g(\mathrm{R}) + 2F_{2g}(\mathrm{R}) + F_{1g} + F_{2u} + 2F_{1u}(\mathrm{IR})$

Hence, in the Raman spectra of spinels only five modes $A_{1g} + E_g + 3F_{2g}$ should be observed. We will use a common notation existing in most of the literature to distinguish between the Raman modes of the same symmetry. The three Raman-active F_{2g} modes are labelled $F_{2g}(1)$, $F_{2g}(2)$, and $F_{2g}(3)$, where $F_{2g}(1)$ is associated with the lowest Raman shift and $F_{2g}(3)$ indicates the Raman F_{2g} symmetry mode at the highest wavenumber.

Before discussing on the comparison among the Raman spectra of the different spinel end-members, we will examine in detail the Raman fingerprint and characteristics of each spinel subgroup, subdivided according to the trivalent cation species (Cr, Al or Fe). Each end-member investigated exhibits a Raman fingerprint with at least one peculiar peak in terms of Raman shift and relative intensity. All the bands observed are then assigned to one of the five predicted modes of given symmetry.

Chromate spinels

Chromate spinels can be described with a general formula $A\mathrm{Cr_2O_4}$.

Raman spectra of three chromate spinels ($ZnCr_2O_4$, $MgCr_2O_4$, and $FeCr_2O_4$) were collected in the range 100-900 cm^{-1} (Fig. 1). The best-fit values for the peak positions are reported in Table 2.

The end-member zincochromite exhibits all the five Raman active modes, whereas both magnesiochromite and chromite end-members show only four Raman bands. Following the literature, these four Raman bands are attributed to the following sequence $E_g < F_{2g}(2) < F_{2g}(3) < A_{1g}$.[31,44] In the zincochromite, the lowest wavenumber band is attributed to the $F_{2g}(1)$ mode in agreement with previous studies.[31,44] The Raman spectra of different chromates show common features: the presence of a group of strong and well-defined bands in the 500 and 700 cm^{-1} range and low-wave number bands below 250 cm^{-1} with weaker or negligible intensity.

It is known that the chromate spinels are all normal spinels with the A^{2+} and Cr^{3+} cations fully ordered in the tetrahedrally and octahedrally coordinated sites, respectively, because Cr^{3+} has a strong preference for the M site. Thus, the chromate spinels give an opportunity to examine how the pure substitution in T sites, made by different divalent cations, affects the vibrational spectra.

The Raman shift of all modes in the chromate spinels changes only by 2-3% with a maximum of 9% for the $F_{2g}(2)$ mode. A negative trend can be observed for the $F_{2g}(2)$ mode with the increase of the tetrahedral cation radius (Fig. 2). Since Bosi et al.[45] stated that the T–O bond lengths are influenced by the cation occupancy at the M site, the tetrahedral cation radii here considered for Mg, Zn and Fe are extracted from the optimized values of $^{T}A^{2+}$-O in chromates reported by Nestola et al.[46] for the Mg cation (0.587 Å), Bosi et al.[45] for the Zn cation (0.591 Å) and Nestola et al.[46] for the Fe^{2+} cation (0.618 Å). The $F_{2g}(2)$ mode has been rarely discussed in literature, but it has been assigned to symmetric bending of the oxygens with respect to the cations in the T sites by some authors.[26,27, 47]

The A_{1g} mode at ~680 cm^{-1} is the strongest mode for all the chromate spinels. Some discrepancies exist on the assignment of this mode. It has been widely attributed to the A^{2+}-O stretching vibration in the T sites.[26-28] However, Malézieux and Piriou[48], Marinković Stanojević et al.[44] Wang et al.[13] and Lenaz and Lughi[21] assigned the Raman band located at about 680 cm^{-1} in their chromate spinels to the symmetric Cr-O stretching vibration of CrO_6 groups. The latter assignment could agree with the strong intensity of the A_{1g} mode observed in our chromate spinels and the small Raman shift variation observed among the different end-members (only 2%).

A careful inspection of the Raman peak position and relative intensity allowed the discrimination among the various end-members.

For its interesting physico-chemical properties, the zincochromite, **$ZnCr_2O_4$**, is commonly used in industrial field for high-temperature ceramic materials, humidity sensors and for catalytic and magnetic materials.[49 and references therein] The Raman spectrum of $ZnCr_2O_4$ shows well-defined and narrow peaks at 182, 452, 511, 605 and 688 cm^{-1} corresponding to all the five Raman-active modes. The peak wavenumbers are in good agreement with previously published experimental and calculated data.[31,44,50,51] The two intense and narrow peaks at 511 and 688 cm^{-1} may be assigned to the $F_{2g}(2)$ and A_{1g} modes, respectively. As in the case of magnesiochromite, the peculiar Raman band is the A_{1g} mode at 688 cm^{-1}. Unlike the magnesiochromite, the zincochromite end-member exhibits the $F_{2g}(2)$ and A_{1g} modes with comparable intensities and a quite strong $F_{2g}(1)$ mode.

Magnesiochromite, **$MgCr_2O_4$**, is a commercially important refractory material and an important component of spinel in upper mantle peridotites. Magnesiochromite is the most common inclusions found in diamonds and very useful to determine the pressure of formation of diamond.[46,52] The Raman spectrum of the $MgCr_2O_4$ end-member shows well-defined and narrow peaks at 446, 542, 612 and 684 cm^{-1} in agreement with the values reported in literature.[21,29,48] The weak $F_{2g}(1)$ mode recorded by Wang et al. [29] at 226.5 cm^{-1} is not detected. Additional bands due to cation disorder or residual Cr_2O_3 from the synthesis are not observed in the investigated spectrum. Magnesiochromite shows the characteristic Raman band corresponding to the A_{1g} mode at 684 cm^{-1}, and a strong $F_{2g}(2)$ mode at 542 cm^{-1}.

Chromite, **$FeCr_2O_4$**, is an important mineral for the production of metallic chromium and occurs in different geological environments, usually within mafic-ultramafic rocks. It is also a ubiquitous mineral in most lunar and Martian meteorites. In addition, chromite is used as refractory material and, since the Bronze Age, as a pigment. In spite of the tangible importance, very few studies on the vibrational properties of chromite spinels have been published and a broad inconsistency exists regarding Raman peak wavenumbers and assignment to specific vibrational modes. The Raman spectrum of the investigated $FeCr_2O_4$ shows features at 436, 493, 591 and 674 cm^{-1} (Fig. 1). The strongest peak at 674 cm^{-1} is the peculiar feature of the end-member chromite and has been assigned to the A_{1g} mode.

Often a variation up to ~40 cm^{-1} of the peak position of all the Raman bands is reported in literature for chromite. For example, the peculiar peak A_{1g} in synthetic pure $FeCr_2O_4$ is relatively sharp and symmetric and is given at ~675 cm^{-1},[21,53] while in natural chromite it is found at higher wavenumbers ~ 680-690 cm^{-1}, with a shoulder at ~ 630 cm^{-1}.[13,54,55] This difference may be due to variation in chemical composition. In fact, Lenaz and Lughi[21] showed that there is a systematic shift of the A_{1g} peak with the increasing of the chromite end-member in the $MgCr_2O_4$-$FeCr_2O_4$ solid solution. A possible correlation between the A_{1g} peak position and the chemical composition of chromite was studied in detail by Wang et al.[13] and Malézieux and Piriou[48]. They observed a systematic shift to higher wavenumbers and a broadening of the A_{1g} mode as the result of increasing primarily the proportion of AlO_6 and secondly of $Fe^{3+}O_6$. Our results are in very good agreement with those reported on single crystal synthetic chromite by Lenaz and Lughi.[21]

Quite controversial in literature is also the assignment of the peaks at low wavenumbers. Wang et al.[13] and Zhang and Gan[55] assigned the peak at 495-520 cm^{-1} to E_g symmetry and the band at 435-450 cm^{-1} to F_{2g} symmetry. However, on the basis of our comparison among the chromate spinels and in agreement with the results reported by Lenaz and Lughi,[21] we attributed these modes to the F_{2g} and E_g symmetry, respectively.

$FeCr_2O_4$ does not show well-defined Raman peaks as those of the other chromate spinels. This difference is due to the dark color which reduces the penetration depth of the excitation laser beam and especially because the Fe-spinels are weaker Raman scatterers than the other spinels.[13] In addition, these authors state that a higher degree of covalency of the bonds provokes higher intensities in the Raman spectrum. In fact, the covalent character of the Cr-O bond in the $MgCr_2O_4$ and $ZnCr_2O_4$ end-members has been demonstrated from the OAS investigation by Hålenius et al.,[38] whereas the very small difference between T-O and M-O bond distances in the end-member $FeCr_2O_4$ measured by Lenaz et al.[56] (T-O = 1.997 Å and M-O = 1.994 Å) suggests that $FeCr_2O_4$ has a more ionic character.

Aluminate spinels

The aluminates with spinel structures present the general formula ACr_2O_4.

Raman spectra of four aluminate spinels ($MgAl_2O_4$, $CoAl_2O_4$, $FeAl_2O_4$ and $MnAl_2O_4$) were collected in the spectral range 150-900 cm^{-1} (Fig. 3). In addition to the Raman spectra here measured, Figure 3 displays the Raman spectrum of a spinel approaching the end-member

gahnite reported by D'Ippolito et al.[42] All aluminates except gahnite exhibit all the five Raman active modes whose wavenumbers are in same sequence as in chromates ($F_{2g}(1) < E_g < F_{2g}(2) < F_{2g}(3) < A_{1g}$).

The aluminates are mainly normal spinel with the A^{2+} cation mostly ordered at the T site and Al at the M site, as in the case of end-member gahnite which shows a very low inversion degree.[42] Looking at the different Raman wavenumbers in the aluminates, it is possible to examine the effect of replacing the tetrahedral cation on the Raman bands and thus to assign them to internal vibrations of the AlO_6 octahedra and/or $A^{2+}O_4$ tetrahedra. The differences in the E_g, $F_{2g}(2)$ and A_{1g} mode wavenumbers among the aluminates are approximately only 3-4%. The $F_{2g}(3)$ mode wavenumber varies in a linear way with the tetrahedral cation radius, with a variation of 9%. The $F_{2g}(1)$ mode seems to have a much greater dependence on the divalent cation because in $MgAl_2O_4$ it has a 35% greater wavenumber than the $F_{2g}(1)$ mode of the other aluminates. In effect, most of the literature agrees that the $F_{2g}(1)$ mode is assigned to a complete translation of the AO_4 within the spinel structure [27,47,56]. On the other hand, the A_{1g} mode varies significantly less than the other Raman modes revealing a minor dependence on the type of divalent cation, although many authors attributed this mode to the A^{2+}-O stretching vibration of AlO_4 groups.[26,28,47]

A very good correlation was found between the peak position of the E_g mode and the tetrahedral cation radius (Fig. 4). The tetrahedral cation radii reported in the Figure 4 are extracted from the optimized values of $^{T}A^{2+}$-O in the aluminates reported by Bosi[57] for Zn (0.569 Å); Lavina et al.[58] for Mg (0.586 Å) and Fe (0.62 Å); Bosi et al.[59] for Co (0.594 Å) and Hålenius et al.[60] for Mn (0.67 Å). This mode has been assigned to the asymmetric bending motion of the oxygen atoms within the T sites.[27,47] Hence, despite the movement affects mainly the oxygen atoms, the presence of different divalent cations in the T sites influences the E_g mode.

Although the investigated aluminate spinels are normal spinels, they show low but non negligible inversion values ranging from 0.13 ($CoAl_2O_4$), 0.15 ($FeAl_2O_4$), 0.16 ($MnAl_2O_4$) to 0.24 ($MgAl_2O_4$) as reported by Bosi et al.[59], Andreozzi and Lucchesi[61], Hålenius et al.[60]. The disordering, the presence of vacancies and general defects within the crystal structure can cause a breakdown in the Raman selection rules and subsequently lead to an activation of phonon modes not predicted by group theory. In spite of their low values, the inversion degrees manifested from the aluminate spinels, except $ZnAl_2O_4$, cause the appearance of an additional peak at ca. 700-720 cm^{-1}. This peak has been attributed to A_{1g} character and has been assigned to the Al-O stretching

vibration of AlO_4 groups.[28] A shoulder peak of the E_g mode is also noticed which has been attributed to the bending mode for Al ions in the T sites, and thus to cation disordering, in the previous studies.[28,32,34] In addition, the cation disorder causes a broadening of all the Raman peaks, this is well visible especially in $MgAl_2O_4$, $MnAl_2O_4$ and $FeAl_2O_4$ end-members. For example, the full-width-half-maximum of the E_g mode varies from 11 cm^{-1} in $ZnAl_2O_4$ end-member to 32 cm^{-1} in $MgAl_2O_4$ end-member.

The end-member spinel *s.s.*, **$MgAl_2O_4$**, is one of the most studied spinels as the prototype of the spinel group. However, most of the studies are focused on high pressure and/or temperature effects and the resulting additional bands appear due to cation disorder.[28,32-34] The Raman spectrum of the investigated end-member $MgAl_2O_4$ exhibits four intense and well-defined bands at 308, 408, 670 and 768 cm^{-1}. These features are in agreement with the previous measurements and calculations using different models.[26,28,32-34,48,62] The fifth Raman mode, $F_{2g}(2)$, has been experimentally reported at 492 cm^{-1} in one paper,[26] whereas theoretical works described it at ~560-570 cm^{-1}.[33,62] In our $MgAl_2O_4$ Raman spectrum, two weak and not well separated bands are observed at 493 and 562 cm^{-1}. Given that O'Horo et al.[26] investigated synthetic spinels, probably the first peak is related to cation disorder whereas the second one could be the $F_{2g}(2)$ mode for the ordered spinel *s.s.*.
The peculiar peak of the end-member spinel *s.s.* is the E_g mode at 408 cm^{-1}. The shape and width of this mode can give information about the cation disordering.[34]

The end-member **$CoAl_2O_4$** does not exist in nature but it is commonly used as blue pigment in paintings and on ceramics since the Middle Ages and became significant since the discovery of its industrial synthesis route in 1802, known as the Thenard's blue. Hence, the Raman studies on the $CoAl_2O_4$ are mainly focuses on blue pigments.[20,63] The recorded spectrum of the end-member $CoAl_2O_4$ shows all the five expected Raman active modes, at 201, 406, 516, 653 and 755 cm^{-1}. The values of the peak positions are in agreement with those reported in literature.[20,63] The most intense and peculiar peak for the end-member $CoAl_2O_4$ is the $F_{2g}(2)$ mode occurring at 516 cm^{-1} which has been assigned to the Co-O stretching vibration in the tetrahedrally coordinated sites by Bouchard and Gambardella.[20] This peak is usually weak and not well-defined in the other aluminates: this allows an easy identification of Co-bearing spinels.

Despite the end-member hercynite, **$FeAl_2O_4$**, is a common mineral found in many terrestrial and extraterrestrial rocks and used as pigment, for refractory materials or for magnetic applications,

Raman studies on $FeAl_2O_4$ are still lacking. The unique Raman spectrum was reported by Ospitali et al.,[64] collected on the surface of a Roman black gloss. The here recorded Raman spectrum of a synthetic single crystal of hercynite is not well defined but five peaks are noticeable at 189, 400, 504, 617 and 748 cm^{-1}. These values agree with those reported by Ospitali et al.,[64] especially for the modes at highest wavenumber. An additional peak due to the cation disorder occurs at 699 cm^{-1} and a small shoulder of the E_g peak is observed at 366 cm^{-1}. The peculiar peak of end-member hercynite is the broad and intense A_{1g} mode (at 748 cm^{-1}) similar to other iron bearing spinels such as magnetite, maghemite and chromite.[65] Also the $F_{2g}(1)$ mode at 189 cm^{-1} is broad and intense but often it is difficult to record.

Natural spinels approaching the end-member galaxite, **$MnAl_2O_4$**, are rare and found only in few localities in metamorphic, often carbonate-rich rocks, associated with other Mn ore minerals. Manganese-rich assemblages can be used to evaluate the oxydation/reduction conditions of metamorphism, and *P-T* estimates can be obtained from adjacent lithologies.[66] In addition, $MnAl_2O_4$ is important in many application fields such as refractory, optoelectronic and oxidation catalysis.[67 and references therein] We are unaware of previous Raman studies of galaxite. The only Raman spectrum reported in literature is on $MnAl_2O_4$ formed secondarily during the Mn/Al_2O_3 catalyst preparation by Strohmeier and Hercules.[68] The Raman spectrum of the investigated end-member $MnAl_2O_4$ exhibits all the five Raman expected modes at 202, 395, 510, 644 and 775 cm^{-1}. Four peaks are intense, well-defined and narrow, the $F_{2g}(3)$ mode at 644 cm^{-1} is weak but well distinct from the background. An additional weak peak is found at 700 cm^{-1} with A_{1g} symmetry activated by the cation disorder. The strongest peak of the end-member galaxite is the $F_{2g}(1)$ mode at 202 cm^{-1}. For this reason the galaxite can be easily distinguished among the other aluminates which usually show weak $F_{2g}(1)$ modes.

Ferrite spinels

The spinel ferrites with general formula AFe_2O_4 have interesting physical properties and are of technological importance. Raman spectra of two ferrite spinels ($MgFe_2O_4$ and $FeFe_2O_4$) were collected in the spectral range 150-900 cm^{-1} (Fig. 5). The best-fit values for the peak positions are reported in Table 2. Their Raman spectra have a similar fingerprint characterized by the presence of a strong and well-defined A_{1g} band at approximately 670-700 cm^{-1} range and weaker bands at lower wavenumbers.

Many ferrites present inverse spinel structure, in which all A^{2+} cation occupy the M sites and the Fe^{3+} cations are distributed almost equally between the T and M sites. In particular, the magnetite spinel, usually, has a completely inverse structure and the investigated magnesioferrite has an inversion degree, calculated on the basis of the structural data reported by Andreozzi et al., [36] equal to 0.89. Hence, looking at the different Raman wavenumbers in the ferrites, it is possible to examine the effect of replacing the divalent cation in the M sites on the Raman bands and thus to obtain information about the internal vibrations of the $A^{2+}O_6$ octahedra and/or $Fe^{3+}O_4$ tetrahedra. This assignment is important in the ferrite spinels because the cation composition and distribution among the T and M sites strongly influence most of their physical properties.

Notice that magnesioferrite shows higher Raman wavenumber values than those of magnetite owing to the large difference of the octahedral Mg and Fe radii ($^{M}Fe^{2+}$ = 0.77 Å and ^{M}Mg = 0.70 Å from Lavina et al.[58]).

The end-member magnesioferrite, **$MgFe_2O_4$**, is an important ferrite usually used as brown pigment, ferrimagnets and dehydrogenation catalysts thanks its chemical and physical properties.[30] $MgFe_2O_4$ natural mineral is uncommon but is recognized as an important component of magnetic spherules extracted from Cretaceous/Tertiary (K/T) sediments. [69] Rare Raman studies on $MgFe_2O_4$ are found in literature and recently they are focused on the determination of the cations' distribution in spinel series.[70,71]

The recorded spectrum of the end-member $MgFe_2O_4$ shows more than the five expected Raman active modes, at 214, 332, 377, 479, 550, 596, 661 and 707 cm^{-1} (Fig. 5). The extra bands are caused by disorder effects of Mg^{2+} and Fe^{3+} over the T and M sites and are strongly consistent with recent data on magnesioferrite.[21,30,70-72]

The broad and strong band at ~710 cm^{-1} is the characteristic Raman feature of the end-member magnesioferrite. As already seen for the other end-members, this peak has an A_{1g} character and is mainly associated to the motion of oxygen atoms in the T sites. Since magnesioferrite doesn't have a completely inverse structure, when some Fe^{3+} cations are replaced by Mg^{2+} cations in the T sites, the A_{1g} mode is split into two bands producing a shoulder at 661 cm^{-1}. Nakagomi et al.[70] and da Silva et al.,[72] considering the large mass difference between Mg and Fe^{3+} cations, stated that the A_{1g} Raman mode at ~710 cm^{-1} is associated to the stretching mode of the $^{T}Fe^{3+}$-O and the A_{1g} Raman mode at ~670 cm^{-1} is associated to the stretching mode of the ^{T}Mg-O. In fact, they demonstrated that in their spinel series the integrated intensities of the A_{1g}(Mg) and A_{1g}(Fe) Raman modes are, respectively, proportional to ^{T}Mg-O and ^{T}Fe-O and they used the

corresponding integrated intensities (I_{Mg}) and (I_{Fe}) to assess the Mg- and Fe-content in the A-site.[72] For the assignment of the other peaks the literature is rather inconsistent. Taking into consideration the magnetite Raman spectrum, which has a completely inverse spinel structure, the Raman bands observed at 214, 332, 479, 550 cm^{-1} could be attributed respectively to the $F_{2g}(1)$, E_g, $F_{2g}(2)$ and $F_{2g}(3)$ Raman mode involving motions of the Fe^{3+} cations. Hence, in agreement with the large mass difference of Mg and Fe^{3+} cations, the Raman bands observed at 377 and 596 cm^{-1} could be assigned to the E_g and $F_{2g}(3)$ Raman mode involving motions of the Mg cations.

The end-member magnetite, **$FeFe_2O_4$**, is a common ferrite spinel from a geological and technological point of view widely used both as mineral carrier of the permanent magnetism in rocks and also as ferromagnetic material especially in the iron metallurgical electro-optical industry. Thanks to its importance, magnetite has been extensively investigated by Raman spectroscopy.[47 and references therein] Raman results from these studies vary significantly either in the number of expected Raman modes or with respect to their positions and assignments.

Raman spectrum of magnetite was conducted on the polished octahedral {111} face of the single crystal of a natural sample. The spectrum shows the characteristic fingerprint composed by three distinct peaks at 312, 548 and 677 cm^{-1}. In addition, a weak peak at 474 cm^{-1}, usually not easily observed in a Raman pattern, was measured. The resulting values are in good agreement with those reported in literature. [47,73-76] Previous assignments of a Raman mode to every band were unclear and/or conflicting. We decided to assign the Raman modes in accord to the results of Shebanova and Lazor,[47] which performed extensive polarized Raman measurements to fill the existing gap. Hence, the bands at 312 and 548 cm^{-1} have an E_g and $F_{2g}(3)$ character and have been assigned to the symmetric and asymmetric bending of oxygen with respect to Fe in the T sites, respectively. The band at 474 cm^{-1} has a $F_{2g}(2)$ character and has been attributed to asymmetric stretch of Fe and O in the T sites and the band at 677 cm^{-1} has a A_{1g} character and has been assigned to the symmetric stretching of oxygen atoms along $^{T}Fe–O$ bonds.

The A_{1g} band is the characteristic Raman feature of the end-member magnetite and it appears as a symmetric peak unlike that observed in the end-member magnesioferrite. The A_{1g} band position in the published results varies between 663 cm^{-1} and 706 cm^{-1}. Different composition in term of minor elements could be the cause of this small shift of the peak position. Another reason of the variable A_{1g} band position could be due to transformation of the magnetite if laser power is too high. In fact, under heating magnetite is transformed first into maghemite (γ -Fe_2O_3) at ~200 ◦C

and then into hematite (Fe_2O_3) at ~400 ◦C. [76] Thus, the variation of the A_{1g} band position might be caused by different laser wavelengths and powers used by different research groups.

In our magnetite, the transformation into the hematite can be excluded by the absence of its very characteristic doublet at ca. 220–280 cm^{-1}. Raman discrimination between magnetite and maghemite is often difficult because the Raman signature of maghemite consists of a strong ca. 670 cm^{-1} peak as the magnetite.[76] However, Hanesch [65] stated that the Raman spectra of magnetite and maghemite can be distinguished by the double peak of maghemite at ~ 710 cm^{-1} and by the 1330 cm^{-1} band, which does not appear in magnetite. The narrow (FWHW ~ 35 cm^{-1}) and rather symmetric peak measured at 677 cm^{-1} in our Raman spectrum of magnetite and the absence of a shoulder on the higher wavenumber side lead to exclude a maghemite phase.

Comparative analysis of the end-member spinels Raman spectra

On the basis of a comparative inspection of the spectra and of the values of the Raman peak positions (Fig. 6), it has been possible to distinguish whether a spinel belongs to the aluminate ($A Al_2O_4$) or to the chromite ($A Cr_2O_4$) or to the ferrite ($A Fe_2O_4$) subgroups. Since the $F_{2g}(1)$ Raman bands are often absent or difficult to measure, they were not considered in the comparison. Where the $F_{2g}(1)$ Raman band was observed, it is located at ~200 cm^{-1} in each end-members with the exception of the spinel *s.s.* where it is found at ~300 cm^{-1}. The $F_{2g}(1)$ Raman mode has been assigned to translation of the whole tetrahedron. [27,47,53] Thus, the higher peak position of the spinel *s.s.* than the other end-members is only due to a lightest atomic mass of Mg with respect to the other divalent cations. Hence, an influence of the octahedral cation on $F_{2g}(1)$ peak position seems to be excluded. The $F_{2g}(2)$ Raman bands occur almost at the same positions in the three sub-groups confirming the assignment to motion of cations occupying only the tetrahedron.

The main difference between the aluminates, chromates and ferrites concerns the A_{1g}, $F_{2g}(3)$ and E_g modes. In fact, these three modes have been assigned to different movements of the oxygen atoms along the T-O bond. Each tetrahedron shares an oxygen with three octahedra, thus, even if the octahedral cation remains at rest, the nature of the M cation must influence the M-O bonding force and cause a change of the oxygen position along the M-O-T direction.

The chromates and ferrites exhibit an intense A_{1g} mode at ~680 cm^{-1}, at lower wavenumbers than the aluminates (~750-770 cm^{-1}), as expected due to the heavier atomic mass of Cr and Fe with respect to Al. The same trend can be seen for the $F_{2g}(3)$ peak position, which changes from 650-660 cm^{-1} in the aluminates to 590-600 cm^{-1} in the chromates and ferrites. Comparing the values of the $F_{2g}(3)$ peak position in MgB_2O_4 and FeB_2O_4 spinels (B = Cr, Al, Fe^{3+}), a good linearly decreasing trend of the $F_{2g}(3)$ wavenumbers with increase of the octahedral cation radii was observed (Fig. 7). Generally, this mode has been assigned to the asymmetric bending or stretching of oxygen with respect to tetrahedral cation,[26,27,47] but the observed trend indicates that the $F_{2g}(3)$ mode is related to the nature of the octahedral cation.

When E_g mode is separately observable, it seems to be the fundamental mode to distinguish an end-member spinel showing a peak position variation up to over 100 cm^{-1} and the unique mode able to discriminate between chromates and ferrites. The Figure 8 shows a clear discrimination of the E_g value among the three sub-groups from ~450 cm^{-1} for the chromates to ~300 cm^{-1} for the ferrites. In addition, each spinel sub-group shows a decrease of the E_g values with the increase of the mean cation radius, that is the average of the tetrahedral and octahedral cation radii in the asymmetric unit composed of two octahedra and a tetrahedron. Hence, the E_g peak position is affected by the type of the cations occupying the T and M sites and can identify the spinel sub-group and also the spinel end-members.

Conclusions

Raman investigation on oxide spinels may be used to obtain chemical information and determine the predominant spinel end-members. Each spinel end-member exhibits a Raman fingerprint with at least one peculiar peak in terms of Raman shift and relative intensity. Chromate and ferrite spinels show a strong and well-defined A_{1g} band between 675 and 710 cm^{-1}. Chromate spinels show narrower peaks (~15 cm^{-1}) than those of the ferrite spinels (~35 cm^{-1}) which are characterized by higher cation disorder. Aluminate spinels exhibit dissimilar Raman fingerprint but each end-member has an most intense and diagnostic peak in the spectrum. An intense and narrow $F_{2g}(1)$ mode located at ~200 cm^{-1} is characteristic for $MnAl_2O_4$ end-member. The $MgAl_2O_4$ end-member can be distinguished by an intense E_g mode at 408 cm^{-1}, which becomes asymmetric with the increase of the cation disorder. When the $F_{2g}(2)$ peak stands out in the Raman spectrum, the spinel has definitively a composition approaching to the $CoAl_2O_4$ end-

member. Raman spectrum with an intense $F_{2g}(3)$ mode and a low or absent A_{1g} mode is distinctive of spinel with dominant $ZnAl_2O_4$ composition. The $FeAl_2O_4$ spinel end-member exhibits two broad and intense peaks at ~190 cm^{-1} and 750 cm^{-1} attributed to $F_{2g}(1)$ and A_{1g} modes, respectively.

Noteworthy, simply analysing the E_g peak position, it is possible to obtain information on which sub-group a spinel belongs to, and a careful inspection allows determination of end-member type. In fact, an E_g mode at ~ 450 cm^{-1} is distinctive of chromate spinels, an E_g mode at ~ 400 cm^{-1} is distinctive of aluminate spinels and an E_g mode below 380 cm^{-1} is distinctive of ferrite spinels.

We are confident that results here obtained will be extremely useful in the Gemology, Mineralogy, Astromineralogy, Geology, Cultural Heritage and Materials Science fields, allowing spinel identification directly on hand specimen without any sample preparation.

Acknowledgments

The authors gratefully acknowledge L. Mantovani, I. Aliatis and E. Lambruschi of the Physics and Earth Sciences Department, University of Parma, for precious technical assistance during the Raman analysis and M. Serracino during EMP data collection. F. Bosi is thanked for his support and helpful comments about the cation distribution. The present study benefited from financial support from the "Progetto Sapienza Avvio alla Ricerca 2014".

References

[1] K.E. Sickafus, J.M. Wills, N.W. Grimes, *J. Am. Ceram. Soc.* **1999**, *82*, 3279-3292.

[2] C. Biagioni, M. Pasero, *Am. Mineral.* **2014**, *99*, 1254-1264.

[3] S.J. Shukla, K.M. Jadhav, G.K. Bichile, *J. Magn. Magn. Mat.* **1999**, *195*, 692-698.

[4] A.L. Fernandez, L. De Pablo, *Pigm. Resin Technol.* **2002**, *31*, 350-356.

[5] G. Fierro, M.L. Jacono, R. Dragone, G. Ferraris, G.B. Andreozzi, G. Graziani, *Appl. Catal. B: Environ.* **2005**, *57*, 153-165.

[6] N.N. Gedam, P.R. Padole, S.K. Rithe, G.N. Chaudhari, *J. Sol-Gel Sci. Techn.* **2009**, *50*, 296-300.

[7] C. Ballhaus, R.F. Berry, D.H. Green, *Contrib. Mineral. Petr.* **1991**, *107*, 27-40.

[8] R.O. Sack, M.S. Ghiorso, *Am. Mineral.* **1991**, *76*, 827-847.

[9] A. Della Giusta, S. Carbonin, G. Ottonello, *Mineral. Mag.* **1996**, *60*, 603-616.

[10] F. Princivalle, A. Della Giusta, A. De Min, E.M. Piccirillo, *Mineral. Mag.* **1999**, *63*, 257-262.

[11] J.J. Papike, P.V. Burger, A.S. Bell, L. Le, C.K. Shearer, S.R. Sutton, J. Jones, M. Newville, *Am. Mineral.* **2013**, *98*, 2193-2196.

[12] C. Perinelli, F. Bosi, G.B. Andreozzi, A.M. Conte, P. Armienti, *Am. Mineral.* **2014**, *99*, 839-846.

[13] A. Wang, K.E. Kuebler, B.L. Jolliff, L.A. Haskin, *Am. Mineral.* **2004**, *89*, 665-680.

[14] L.E. Mayhew, E.T. Ellison, T.M. McCollom, T.P. Trainor, A.S. Templeton, *Nature Geosci*. **2013**, *6*, 478-484.

[15] K. Righter, L.R. Danielson, K. Pando, R.V. Morris, T.G. Graff, D.G. Agresti, A.M. Martin, S.R. Sutton, M. Newville, A. Lanzirotti, *Am. Mineral.* **2013**, *98*, 616-628.

[16] J.E. Shigley, C.M. Stockton, *Gems Gemol.* **1984**, *20*, 34-41.

[17] A.K. Malsy, S. Karampelas, D. Schwarz, L. Klemm, T. Armbruster, D.A. Tuan, *J. Gemmol.* **2012**, *33*, 19-27.

[18] D. de Waal, *J. Raman Spectrosc.* **2009**, *50*, 296-300.

[19] S. Saeseaw, W. Wang, K. Scarratt, J.L. Emmett, T.R. Douthit GIA. **2009**, *1*. Available at: http://www.gia.edu/researchresources/newsfromresearch/Heated%20spinel%20Identification%20at%20April%2002%202009.pdf.

[20] M. Bouchard, A. Gambardella, *J. Raman Spectrosc.* **2010**, *41*, 1477-1485.

[21] D. Lenaz, V. Lughi, *Phys. Chem. Miner.* **2013**, *40*, 491-498.

[22] RRUFF Project. Department of Geosciences, University of Arizona, Tucson, USA. Available at: http://rruff.info/ (accessed March 2015).

[23] Minerals Raman Database. Physics Department, University of Parma, Italy. Available at: http://www.fis.unipr.it/phevix/ramandb.html (accessed March 2015).

[24] Handbook of Minerals Raman Spectra. Ecole normale supérieure de Lyon, Lyon. Available at: http://www.ens-lyon.fr/LST/Raman/ index.php. (accessed March 2015).

[25] RASMIN, Raman Spectra Database of Minerals and Inorganic Materials. National Institute of Advanced Industrial Science and Technology (AIST), Japan. Available at: http://riodb.ibase.aist.go.jp/rasmin/ (accessed March 2015).

[26] M.P. O'Horo, A.L. Frisillo, W.B. White, *J. Phys. Chem. Solids* **1973**, *34*, 23-28.

[27] J.L. Verble, *Phys. Rev. B* **1974**, *9*, 5236-5248.

[28] H. Cynn, S.K. Sharma, T.F. Cooney, M. Nicol, *Phys. Rev. B* **1992**, *45*, 500-502.

[29] Z. Wang, H.S.C. O'Neill, P. Lazor, S.K. Saxena, *J. Phys. Chem. Solids* **2002**, *63*, 2057-2061.

[30] Z. Wang, P. Lazor, S.K. Saxena, H.S.C. O'Neill, *Mater. Res. Bull.* **2002**, *37*, 1589-1602.

[31] Z. Wang, P. Lazor, S.K. Saxena, G. Artioli, *J. Solid State Chem.* **2002**, *165*, 165-170.

[32] N.V. Minh, I.S. Yang, *Vib. Spectrosc.* **2004**, *35*, 93-96.

[33] M. Lazzeri, P. Thibaudeau, *Phys. Rev. B* **2006**, *74*, 140301.

[34] S.P. Slotznick, S.H. Shim, *Am. Mineral.* **2008**, *93*, 470-476.

[35] D. Errandonea, in *AB_2X_4 Chalcogenide Compounds*, (Springer Series in Materials Science 189), Springer-Verlag Berlin Heidelberg, **2014** E. Wiley.

[36] G.B. Andreozzi, F. Bosi, F. Garramone, *Period. Mineral.* **2001**, *70*, 193-204.

[37] U. Hålenius, F. Bosi, H. Skogby, *Am. Mineral*. **2007**, *92*, 1225.

[38] U. Hålenius, G.B. Andreozzi, H. Skogby, *Am. Mineral.* **2010**, *95*, 456-462.

[39] M. Quintiliani, G.B. Andreozzi, H. Skogby, *Period. Mineral.* **2011**, *80*, 39-55.

[40] V. D'Ippolito, G.B. Andreozzi, F. Bosi, U. Hålenius, *Am. Mineral.* **2012**, *97*, 1828-1833.

[41] J.C. Gaspar, P.J. Wyllie, *Am. Mineral.* **1983**, *68*, 195-213.

[42] V. D'Ippolito, G.B. Andreozzi, F. Bosi, U. Hålenius, L. Mantovani, D. Bersani, R.A. Fregola, *Mineral. Mag.* **2013**, *77*, 2941-2953.

[43] W.B. White, B.A. DeAngelis, *Spectrochim. Acta A-M.* **1967**, *23*, 985-995.

[44] Z.V. Marinković Stanojević, N. Romčević, B. Stojanović, *J. Eur. Ceram. Soc.* **2007**, *27*, 903-907.

[45] F. Bosi, G.B. Andreozzi, U. Hålenius, H. Skogby *Am. Mineral.* **2011**, 96, 594-598.

[46] F. Nestola, B. Periotto, G.B. Andreozzi, E. Bruschini, F. Bosi, *Am. Mineral.* **2014**, *99*, 1248-1253.

[47] O.N. Shebanova, P. Lazor, *J. Solid State Chem.* **2003**, *174*, 424-430.

[48] J.M. Malézieux, B. Piriou, *Raman. B. Minéral.* **1988**, *111*, 649−669.

[49] N. Singh, J.Y. Rhee, *J. Korean Phys. Soc.* **2010**, *57*, 1233-1237.

[50] H.C. Gupta, M.M. Sinha, Balram, B.B. Tripathi *J. Solid State Chem.* **1993**, *102*, 315-317.

[51] C. Kant, J. Deisenhofer, T. Rudolf, F. Mayr, F. Schrettle, A. Loidl, V. Gnezdilov, D. Wulferding, P. Lemmens, V. Tsurkan, *Phys. Rev. B* **2009**, *80*, 214417.

[52] D. Lenaz, A.M. Logvinova, F. Princivalle, N.V. Sobolev, *Am. Mineral.* **2009**, *94*, 1067-1070.

[53] B. D. Hosterman, *UNLV Theses/Dissertations/Professional Papers/Capstones.* 2011, pp. 1087. Available at: http://digitalscholarship.unlv.edu/thesesdissertations/1087.

[54] M. Chen, J. Shu, X. Xie, H.K. Mao, *Geochim. Cosmochim. Ac.* **2003**, *67*, 3937-3942.

[55] Z.W. Zhang, F.X. Gan, *J. Raman Spectrosc.* **2011**, *42*, 1808-1811.

[56] D. Lenaz, H. Skogby, F. Princivalle, U. Hålenius, *Phys. Chem. Miner.* **2004**, *31*, 633-642.

[57] F. Bosi, *Acta Crystallogr. B* **2014**, *70*, 697-704.

[58] B. Lavina, G. Salviulo, A.D. Giusta, *Phys. Chem. Miner.* **2002**, *29*, 10-18.

[59] F. Bosi, U. Hålenius, V. D'Ippolito, G.B. Andreozzi, *Am. Mineral.* **2012**, *97*, 1834-1840.

[60] U. Hålenius, F. Bosi, H. Skogby, *Am. Mineral.* **2011**, *96*, 617-622.

[61] G.B. Andreozzi, S. Lucchesi, *Am. Mineral.* **2002**, *87*, 1113-1120.

[62] G.A. de Wijs, C.M. Fang, G. Kresse, G. de With, *Phys. Rev. B* **2002**, *65*, 094305.

[63] L.D. Kock, D. de Waal, *J. Raman Spectrosc.* **2007**, *38*, 1480-1487.

[64] F. Ospitali, T. Sabetta, F. Tullini, M.C. Nannetti, G. Di Lonardo, *J. Raman Spectrosc.* **2005**, *36*, 18-23.

[65] M. Hanesch, *Geophys. J. Int.* **2009**, *177*, 941-948.

[66] E. Gnos, T. Peters, *Contrib. Mineral. Petr.* **1995**, *120*, 372-377.

[67] M. Edrissi, M. Soleymani, M. Naderi, *J. Sol-Gel Sci. Techn.* **2012**, *64*, 485-492.

[68] B.R. Strohmeier, D.M. Hercules, *J. Phys. Chem.* **1984**, *88*, 4922-4929.

[69] F.T. Kyte, J.A. Bostwick, *Earth Planet. Sc. Let.* **1995**, *132*, 113-127.

[70] F. Nakagomi, S.W. da Silva, V.K. Garg, A.C. Oliveira, P.C. Morais, A. Franco Jr, *J. Solid State Chem.* **2009**, *182*, 2423-2429.

[71] B. Antic, N. Jovic, M.B. Pavlovic, A. Kremenovic, D. Manojlović, M. Vucinic-Vasic, A.S. Nikolić, *J. Appl. Phys.* **2010**, *107*, 043525-7.

[72] S.W. da Silva, F. Nakagomi, M.S. Silva, A.Franco Jr., V.K. Garg, A.C. Oliveira, P.C. Morais, *J. Nanopar. Res. C* **2012**, *14*, 1-10.

[73] J. Dünnwald, A. Otto, *Corros. Sci.* **1989**, *29*, 1167-1176.

[74] D. Bersani, PP. Lottici, A. Montenero, *J. Raman Spectrosc.* **1999**, *30*, 355-360.

[75] L.N.D. Bellot-Gurlet, S. Reguer, J. Monnier, M. Saheb, P. Dillmann, *J. Nanopart. Res.* **2009**, *8*, 147-156.

[76] Z. Cvejic, S. Rakic, A. Kremenovic, B. Antic, C. Jovalekic, P. Colomban, *Solid State Sci.* **2006**, *8*, 908-915.

[77] F. Bosi, U. Hålenius, H. Skogby, *Am. Mineral.* **2009**, *94*, 181-189.

Figure captions

Figure 1. Raman spectra of the investigated chromate spinels.

Figure 2. Variation of the $F_{2g}(2)$ mode with the tetrahedral cation radius in the chromate spinels. The size of the symbols used is equal to or larger than standard uncertainties. Dotted line connecting the points is a guide for the eye.

Figure 3. Raman spectra of the investigated aluminate spinels. The observed Raman modes are marked and those due to disordering of the cations are reported with an asterisk.

Figure 4. Variation of the E_g mode with the tetrahedral cation radius in the aluminate spinels. Size of the symbols used is equal to or larger than standard uncertainties. The dotted line connecting the points is a guide for the eye. Solid line is the best fit to experimental data with the equation: $y = 1021x^2 - 1429x + 894$.

Figure 5. Raman spectra of the investigated ferrite spinels.

Figure 6. Comparative variation of the Raman peak positions (cm^{-1}) of the investigated end-member spinels as a function of tetrahedral cation radius and sub-group (aluminates, chromates and ferrites). Dotted lines in color are linear fit to experimental data. Dashed horizontal lines are guides for the eye to help defining the fields of the three sub-groups.

Figure 7. Variation of the wavenumbers of the $F_{2g}(3)$ Raman active modes with the octahedral cation radii in the MgB_2O_4 and FeB_2O_4 spinels with B = Al, Cr and Fe^{3+}. Since the ferrite spinels have an inverse configuration, the octahedral cation radius for the magnesioferrite (0.66 Å) and magnetite (0.68 Å) was obtained subtracting the oxygen radius (O^{2-} = 1.38 Å) to the M-O bond distances reported by Andreozzi et al.[36] and Bosi et al.,[77] respectively. The size of the symbols used is equal to or larger than standard uncertainties. The solid line is the best fit to experimental data.

Figure 8. Variation of the E_g Raman peak positions with the mean cation radius in the three spinel sub-groups. In the calculation of the mean cation radius was considered the various tetrahedral and octahedral cation radii obtained by Andreozzi et al.,[36] D'Ippolito et al.,[42] Nestola et al.,[46] Bosi et al.,[59] Hålenius et al.,[60] Andreozzi and Lucchesi[61] and Bosi et al.[77] in order to consider also the effect of the cation inversion. The size of the symbols used is equal to or larger than standard uncertainties. Solid line is the best fit to experimental data.

Table headings

Table 1. Chemical composition of the investigated spinel samples

Table 2. Measured wavenumbers (in cm^{-1}) for the Raman modes of several end-member spinels

Samples	$MgCr_2O_4$ (MgCr 100B) from Hålenius et al.[38]	$ZnCr_2O_4$ (ZnCr 100) from Hålenius et al.[38]	$FeCr_2O_4$ (FeCr100) from Quintiliani et al.[39]	$MgAl_2O_4$ (Sp3/10a) from Andreozzi et al.[36]	$MnAl_2O_4$ (Gx100) from Hålenius et al.[37]	$FeAl_2O_4$ (He100c/a) from Andreozzi et al.[36]	$CoAl_2O_4$ (CoAl100) from D'Ippolito et al.[40]	$ZnAl_2O_4$ (Ni8967c) from D'Ippolito et al.[42]	$MgFe_2O_4$ (MgF100f/fa) from Andreozzi et al.[36]	$FeFe_2O_4$ This work
MgO (wt.%)	20.7(1)			28.5(3)		0.03(2)		0.03(1)	19.0(2)	4.59(74)
ZnO		34.77(17)						41.7(4)		
MnO					41.35(1)			0.11(3)		0.59(8)
CoO							43.1(3)			
FeO_{tot}			31.9(2)			44.7(2)		2.95(6)	72.6(5)	87.46(1.44)
Al_2O_3	0.08(1)	0.09(5)		71.0(3)	58.73(1)	55.5(4)	55.5(4)	55.5(4)		0.47(40)
Cr_2O_3	78.47(16)	66.32(33)	67.7(3)							
Total	99.24	101.22	99.6	99.5	100.08	100.23	98.6	100.29	91.6	93.11
Cations on the basis of 4 oxygens										
Mg (apfu)	0.994(6)			1.011(6)		0.001(1)		0.001(1)	0.956(8)	0.253(38)
Zn		0.982(5)						0.935(4)		
Mn					1.008(1)			0.003(1)		0.019(2)
Co							1.017(5)			
Fe^{2+}			1.000			0.999(1)		0.062(1)	0.044(8)	0.728(28)
Fe^{3+}						0.092(6)		0.012(1)	2.000(1)	1.979(43)
Al	0.003(0)	0.004(2)		1.992(4)	1.992(1)	1.908(6)	1.989(5)	1.987(3)		0.021(17)
Cr	2.001(4)	2.006(4)	2.000							
Total	2.998	2.995	3.000	3.003	3.000	3.000	3.006	3.000	3.000	3.000

Estimated standard deviation in brackets

Modes	$F_{2g}(1)$	E_g	E_g	$F_{2g}(2)$	$F_{2g}(2)$	$F_{2g}(3)$	$F_{2g}(3)$	A_{1g}	A_{1g}
$ZnCr_2O_4$	182		452		511	605			**688**
$MgCr_2O_4$			446		542	612			**684**
$FeCr_2O_4$			436		493	591			**674**
$ZnAl_2O_4$			*411*		*510*	***661***			
$MgAl_2O_4$	308	*375*sh*	**408**	*493	562	670		*720	768
$CoAl_2O_4$	201		406		**516**	653		*709	755
$FeAl_2O_4$	**189**	*366*sh*	400		504	617		*699	**748**
$MnAl_2O_4$	**202**	*374*sh*	395		510	644		*700	775
$MgFe_2O_4$	*214	*332	377		*479	550	*596	661*sh*	***707**
$FeFe_2O_4$			*312		*474	*548			***677**

sh = shoulder. The modes marked with an asterisk are provoked by the inversion. The peculiar peak of each end-member spinel is marked in bold type face. Raman modes values of $ZnAl_2O_4$ end-member are in italics and are taken from D'Ippolito et al.[42]

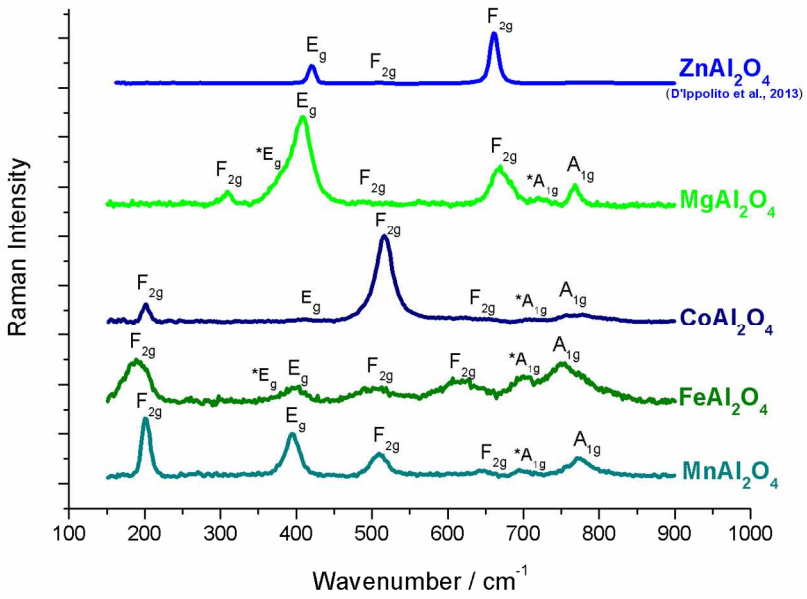

287x199mm (150 x 150 DPI)

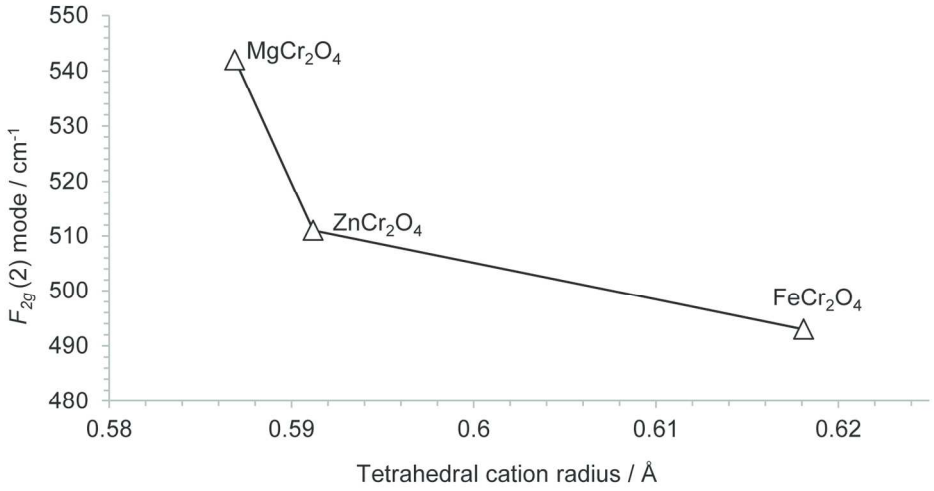

147x76mm (300 x 300 DPI)

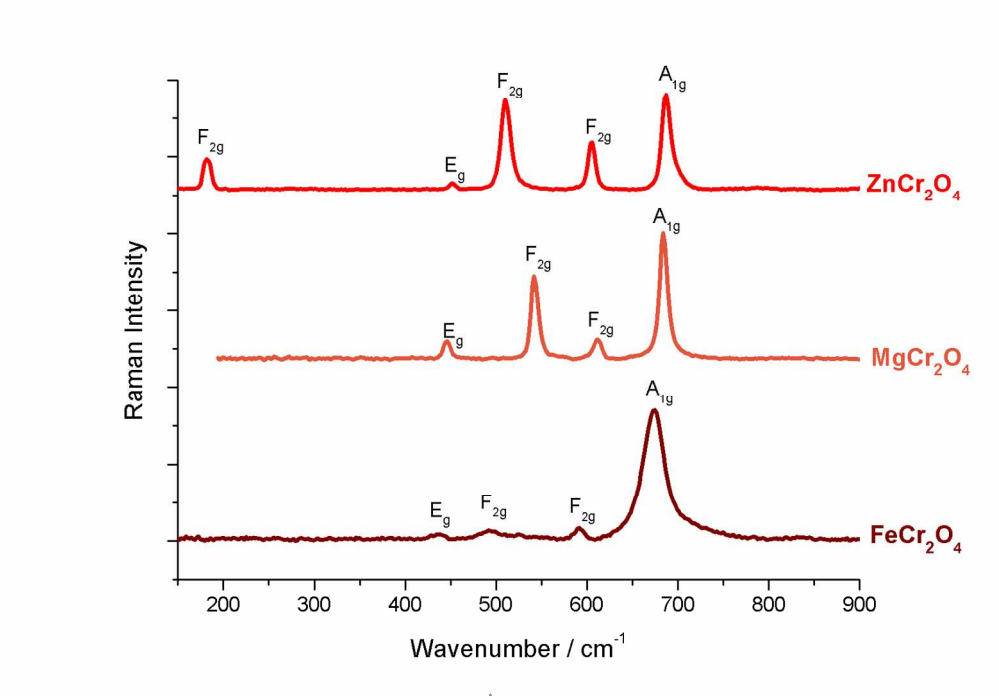

287x199mm (150 x 150 DPI)

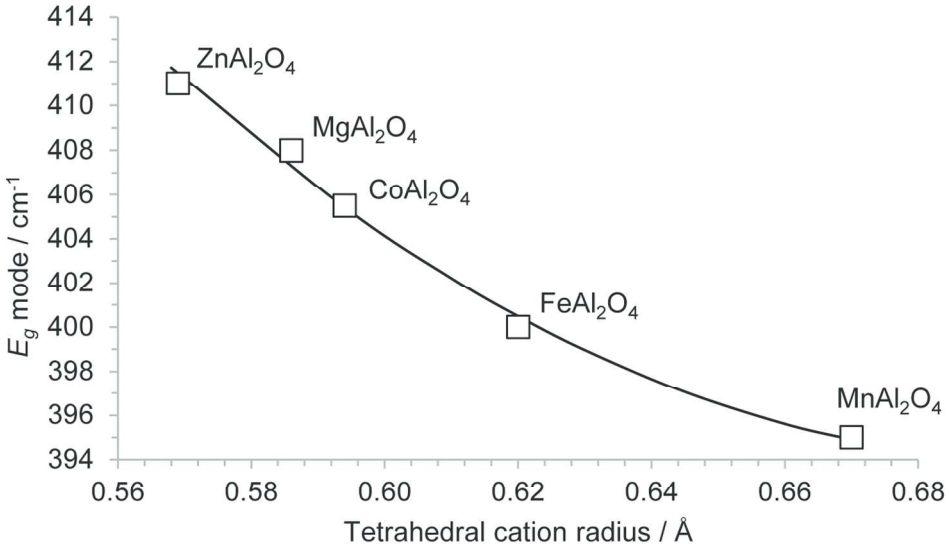

127x76mm (300 x 300 DPI)

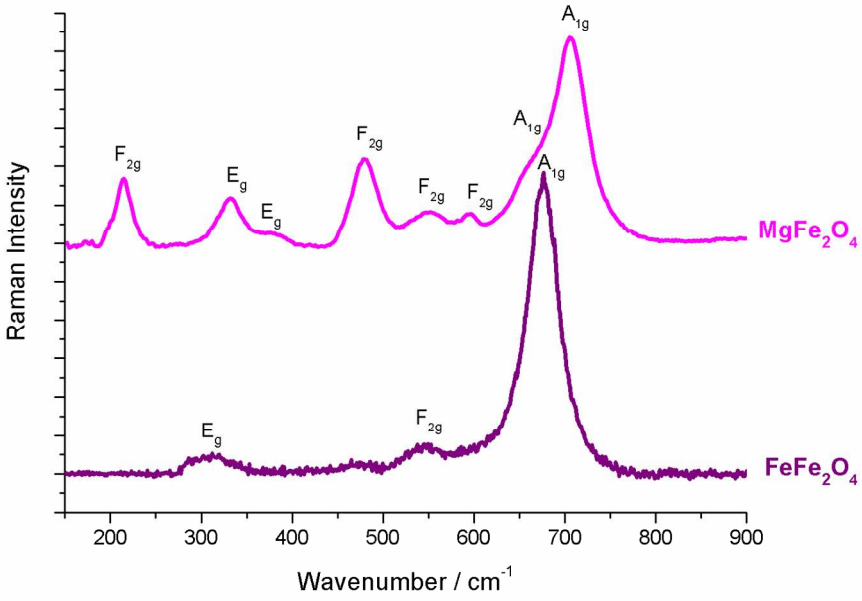

287x199mm (150 x 150 DPI)

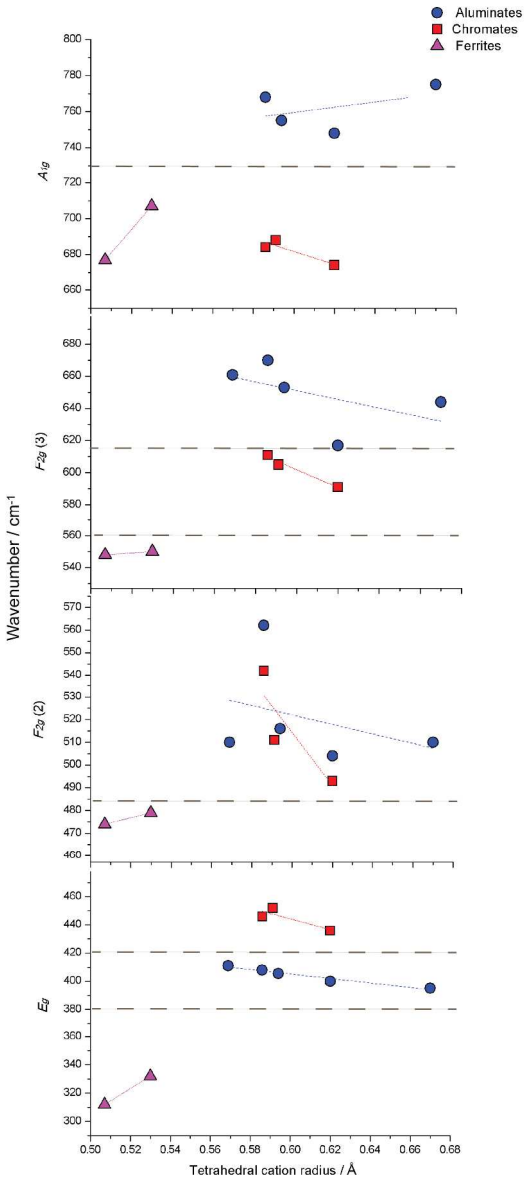

136x301mm (299 x 299 DPI)

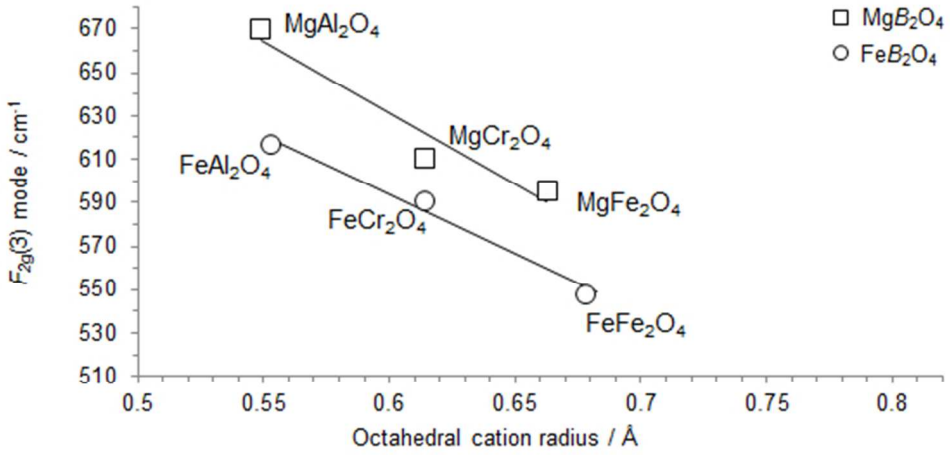

204x101mm (72 x 72 DPI)

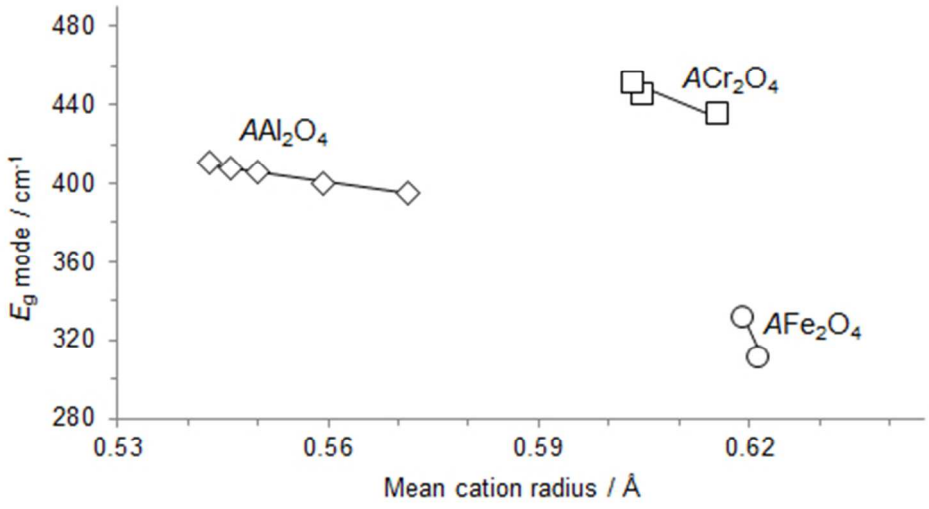

183x101mm (72 x 72 DPI)